REPORT DOCUMENTATION PAGE

AFRL-SR-AR-TR-04-

0065

1. REPORT DATE (DD-MM-YYYY)	2. REPORT TYPE	3. DATES COVERED (From - To)
01/13/2004	Final	01/01/02 - 12/31/03

4. TITLE AND SUBTITLE

Sensor Array Networks for Structural Integrity

5a. CONTRACT NUMBER

5b. GRANT NUMBER
G - F49620-02-1-0139

5c. PROGRAM ELEMENT NUMBER

6. AUTHOR(S)

Jason Speyer

5d. PROJECT NUMBER

5e. TASK NUMBER

5f. WORK UNIT NUMBER

7. PERFORMING ORGANIZATION NAME(S) AND ADDRESS(ES)

University of California, Los Angeles
Mechanical and Aerospace
Engineering Dept. 48-121
Engineering IV, Box 95197
Los Angeles, CA 90095-1597

8. PERFORMING ORGANIZATION REPORT NUMBER

9. SPONSORING / MONITORING AGENCY NAME(S) AND ADDRESS(ES)

USAF, AFRL
4015 Wilson Blvd, Room 713
Arlington, VA 22203-1954

NM

10. SPONSOR/MONITOR'S ACRONYM(S)

11. SPONSOR/MONITOR'S REPORT NUMBER(S)

12. DISTRIBUTION / AVAILABILITY STATEMENT

Approved for public release; distribution unlimited

20040203 015

13. SUPPLEMENTARY NOTES

The views, opinions and/or findings contained in this report are those of the author(s) and should not be constructed as an official U.S. Air Force position,

14. ABSTRACT

In current technologies, given the high reliability required in almost all systems, the ability to detect a system fault at the earliest possible stage is of primary interest. The routine manual inspections required for structures in mechanical, civil, and aerospace fields, significantly increase maintenance costs while also increasing system efficiency and reducing risk. In addition, diagnostic tools can provide information on inaccessible parts in the structure. To provide the necessary architecture for this health maintenance, an array of sensor is used to monitor the system.

15. SUBJECT TERMS

structural health monitoring, fault detection

16. SECURITY CLASSIFICATION OF:			17. LIMITATION OF ABSTRACT	18. NUMBER OF PAGES	19a. NAME OF RESPONSIBLE PERSON
a. REPORT	b. ABSTRACT	c. THIS PAGE	Unlimited		Jason Speyer
					19b. TELEPHONE NUMBER (include area code) (310) 206-4451

Sensor Array Networks for Structural Integrity

Jason L. Speyer

Mechanical & Aerospace Engineering Department

Henry Samueli School of Engineering & Applied Science

University of California, Los Angeles

Los Angeles, California, 90095

Grant No. F49620-02-1-0139

January 12, 2004

1 Objectives

In current technologies, given the high reliability required in almost all systems, the ability to detect a system fault at the earliest possible stage is of primary interest. The routine manual inspections required for structures in mechanical, civil and aerospace fields, significantly increase maintenance cost. Our objective is to develop and implement a self-diagnostic tool that would reduce costs while also increasing system efficiency and reducing risk. In addition, diagnostic tools can provide information on inaccessible parts in the structure. To provide the necessary architecture for this health maintenance, an array of sensor is used to monitor the system.

2 Status of Effort

During this grant, a fault detection filter was developed for structural health monitoring of a simply supported beam. More complex structures would be addressed later. The filter design is based on a mathematical model of the structure and relies on four measurements and one actuation point. Based on structural analysis, the structural damage is decomposed

and reduced to a fault direction vector that maintains a fixed direction in the detection space. We show that this fault detection vector can be detected and uniquely identified and thereby, the structural damage is detected and localized.

3 Accomplishments/New Findings

During this grant, robust fault detection filter based on a spectral design method is implemented for a simply supported beam and is shown to both identify and localize structural faults. See Appendix A for details. The algorithm is specifically accomplished using 4 sensors and 1 actuator and relays on a mathematical model of the structure. The detection filter design is based on fault direction vectors that can be uniquely associated with any structural fault occurring at the beam. At each damage locations the detection filter measurement residual vector produces a fixed direction independent of the fault (damage) size that can be uniquely identified. The numerical simulations are compared with experimental results produced by an aluminum simply supported beam and show good agreement. The measurements and actuation of the beam are obtained with piezoelectric transducers that ensure a large operating bandwidth. Although the algorithm is designed specifically for 4 measurements, it can be adapted to virtually any number of sensors. This is a fundamental properties for structural health monitoring because, depending on structure complexity, the damage detection must be accomplished using the least number of sensors. The fault-detection filter methodology can also include sensors and actuator faults, as well as plant faults as addressed here. However, in this grant period, only structural faults are considered.

For the implementation of the fault detection filter, the following equipments where utilized: 1) A Wavetek 10MHz DDs Mod. 29 function generator to produce the sinusoidal inputs for the actuator, 2) a low impedance Burleigh PZ 150M volt amplifier for the amplification of the actuator input, and 3) a National Instruments PCI-MIO-16E-1 PC card for data acquisition. The data from the sensors and actuator were sampled at 40 Ksample/sec and each acquisition lasted asted 10 seconds. In order to reduce the noise effect, digital Chebychev low pass and band-pass filter where appropriately designed for each of the input

and output signals. The state integration was obtained with a Runge-Kutta fourth order method using Matlab software. The actuator input was approximately 120 Volts after amplification and the average output from the sensors was approximately 2 Volts[1]. The norms of the projected residuals obtained from the undamaged structure had magnitude of approximately 10^{-2}, indicating good tracking of the filter.

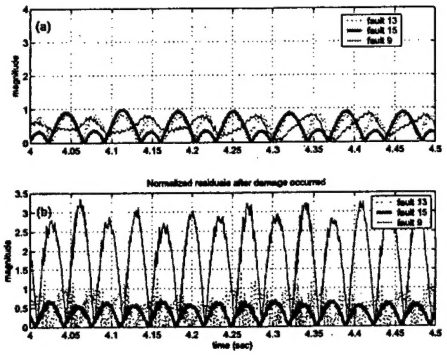

(a) Filter N^o1

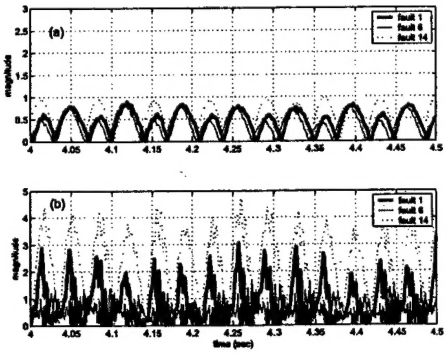

(b) Filter N^o4

Figure 1: Measured data. Filter N^o 1 and Filter N^o 4. Normalized norms of the projected residuals: A) Before damage and B) after damage

[1]The average measured capacitance of each sensor is $C \cong 3nF$ resulting in high impedance and thereby high voltage output even with small currents generally experienced with piezoelectric transducers.

The damage inflicted upon the structure was a saw cut of approximately 5mm $\times$ 1 mm made on one side of the beam at approximately 448 mm from the beam left-hand edge. The saw cut position was chosen coincident with the pre-defined fault location N^o 9. A new set of data was taken from the damaged structure and compared with the estimate of the fault detection filter. The resulting norms of the projected residuals are shown in figure (1) for filter N^o 1 and filter N^o 4, respectively. Recall that, for this scenario, filter N^o 1 is the filter that supposedly should detect the damage. In the figure, for each filter, in case A) are shown the normalized norms of residuals before damage occurs and in case B) are shown the normalized norms of residuals after damage has occurred. The residuals are normalized with respect to values obtained before damage had occurred. As it can be seen from figure (1), in both filters, when there was no damage, all the three residuals have similar values. After damage occurred, in filter N^o 1, the norm of the pre-defined fault direction, location 9, increased approximately 3 times while the other two norms, location 13 and 15, were essentially unchanged. This indicated that the projector 9 detected a damage coincident with the fault location 9. For filter N^o 4, instead, all the residual norms increased indicating that no specific fault was detected. Although not shown, the residual norms of filter N^o 2, 3 and 5, after damage had occurred, showed a behavior similar to the one of filter N^o 4 indicating that no specific fault was detected.

4 Personnel Supported

Personnel supported or associated with this grant are:

- Professors
  - Jason L. Speyer
  - Gregory Carman
- Graduate Students
  - Sauro Liberatore Received Ph.D.

– Andy Chunliang Hsu m.s.

5 Publications

Sauro Liberatore, Jason L. Speyer and Andy Chunliang Hsu, Fault detection filter applied to structural health monitoring," Proceedings of the IEEE Conference on Decision and Control, Dec. 2003.

6 iteractions/transitions

The following meetings were attended:

- Test and Evaluation Program Review 02
- Test and Evaluation Program Review 03
- IEEE Conference on Decision and Control, Dec. 2003.

7 New Discoveries, Inventions, or Patent Disclosures

None

8 Honors/Awards

Jason L. Speyer:

- Fellow of the IEEE and AIAA.
- Recipient of the IEEE Third Millennium Medal
- Department of the Air Force Award for Meritorious Civilian Service, 2001
- NASA Public Service Group Achievement Award awarded to the UCLA Autonomous Vehicles System Instrumentation Laboratory 2002

Appendix A

Fault Detection Filter Applied to Structural Health Monitoring

Fault detection filter applied to structural health monitoring

Sauro Liberatore, Jason L. Speyer and Andy Chunliang Hsu

Mechanical & Aerospace Engineering Department

Henry Samueli School of Engineering & Applied Science

University of California, Los Angeles

Los Angeles, California, 90095

Email: sauro@seas.ucla.edu, speyer@seas.ucla.edu, chunlian@seas.ucla.edu

January 12, 2004

Abstract

In this paper, a fault detection filter is developed for structural health monitoring of a simply supported beam. The filter design is based on a mathematical model of the structure and relies on four measurements and one actuation point. Based on structural analysis , the structural damage is decomposed and reduced to a fault direction vector that maintains a fixed direction in the detection space. According to detection filter theory, this fault detection vector can be detected and uniquely identified and thereby, the structural damage is detected and localized. The design algorithm uses an eigenstructure assignment approach which allows accommodation of ill-conditioned eigenvectors in the construction of the gains. For this particular design, 15 pre-defined fault positions are simulated so that the corresponding fault direction vectors are utilized as basis to identify any of the infinite possible damage locations. The design required 5 fault detection filters each of one using 3 of the 15 pre-defined fault locations. The filter is applied to the data obtained from experimental results of an aluminum simply supported beam with 4 piezoelectric sensors and 1 piezoelectric actuator. In particular, by exciting the structure at the first natural frequency, a 3.5 mm saw cut made to one side of the aluminum beam, is detected and localized.

1 Introduction

In current technologies, given the high reliability required in almost all systems, the ability to detect a system fault at the earliest possible stage is of primary interest. The routine manual inspections required for structures in mechanical, civil and aerospace fields, significantly increase maintenance cost. Implementing a self-diagnostic tool would reduce costs while also increasing system efficiency and reducing risk. In addition, diagnostic tools can provide information on inaccessible parts in the structure. Damage detection is therefore, an important asset. A system that continuously monitors a structure in order to detect damage, is often referred to as a health monitoring system. While the potential payoffs are high, developing a reliable technique to monitor damage evolution in a structure is a difficult task to achieve. In past decades, many different approaches have been proposed and among them, the updated modal parameter methods are the most prominent. The idea of utilizing updated modal parameters for health monitoring approaches is as follow. Suppose that the finite element model (FEM) of the structure has been refined and validated by test data prior to damage. Next, assume at some later date, structural damage has occurred and a new set of data has been taken. Then, the discrepancies between the new set of acquired data and the previous refined FEM model, generally resulting in a matrix of sparse data, can be used to locate the damage. The baseline of these techniques utilize iterative algorithms to identify differences either in the stiffness matrix or in the flexibility matrix prior to and following damage. A review of these health monitoring methods can be found in reference [1] while some interesting results along with some generic issues and limitations are found in reference [2]. The limiting issues of all these techniques are related to the iterative algorithm and its numerical error that can overtake the small differences obtained between the update matrices and the baseline and thereby lowering the method sensitivity to damage. In addition, a possible sensor or actuator fault cannot be included in the analysis and could rase misleading conclusions.

An alternative approach can be obtained by using the fault detection filter theory that creates an estimated output based on a baseline structural model. The filter residual, com-

posed of the difference between the estimated output and the measured one, is constructed to have an invariant direction in the presence of an element from a set of *a priori* faults which allows both detection and identification. The fault detection filter was first introduced by [3] and refined by [4] and is also known as Beard-Jones detection filter. A spectral analysis of the Beard-Jones detection filter and an improved design algorithm have been developed in [6]. Furthermore, an important geometric interpretation of the Beard-Jones detection filter has been developed in [5]. Based on this geometric interpretation, a new fault detection filter, called restricted diagonal detection filter, has been generalized from the Beard-Jones detection filter [5]. Finally, design algorithms have been developed to improve the robustness of both fault detection filters [7,8]. In particular, the spectral method of [7] is applied here. The filter effectiveness has been proved in a number of practical applications such as sensor and actuator faults in automotive systems, references [9] and [10], and for GPS/INS navigation system, reference [11]. However, very few applications of structural health monitoring can be found in literature. Probably, the first example was presented by Mehra and Peshon (1970), [12], that proposed a Kalman filter to estimate the changes in the time domain of a faulty system. Among other possible applications, fault detection for an aircraft jet engine is included, even though no specific algorithm was provided. A more recent example is found in Waller and Schmidt (1999), [13], where system identification through an extended Kalman filter is used. The idea is to update the filter and identify the changes in the system parameters. By using an analytical model and tracking the updated parameters, the fault can be localized. The proposed approach relies on single frequency shifts that are generally very small and therefore highly affected by instrumentation error. Another approach is proposed by Fritzen and Mengelkamp (2002), [14], that utilized a vibration based, time-domain method with a Kalman filter that detects fault by the increase of covariances from the residuals. From the statistical evaluation, one can then setup a threshold to judge the degree of significance in the observed changes and determine whether the changes are indeed resulted from damage in the system or disturbances due to noise. The approach is implemented for a composite panel with stringers and it is shown effective in detecting damage even though the method is incapable of damage localization.

In this paper, the fault detection filter [7] is implemented for a simply supported beam and is shown to both identify and localize structural faults. The algorithm is specifically accomplished using 4 sensors and 1 actuator and relays on a mathematical model of the structure. The detection filter design is based on fault direction vectors that can be uniquely associated with any structural fault occurring at the beam. At each damage locations the detection filter measurement residual vector produces a fixed direction independent of the fault (damage) size that can be uniquely identified. The numerical simulations are compared with experimental results produced by an aluminum simply supported beam and show good agreement. The measurements and actuation of the beam are obtained with piezoelectric transducers that ensure a large operating bandwidth. Although the algorithm is designed specifically for 4 measurements, it can be adapted to virtually any number of sensors. This is a fundamental properties for structural health monitoring because, depending on structure complexity, the damage detection must be accomplished using the least number of sensors. The fault-detection filter methodology can also include sensors and actuator faults, as well as plant faults as addressed here. However, in the present paper, only structural faults are considered.

2 Fault Detection Filter. General Theory

Consider a linear time invariant system

$$\begin{aligned} \dot{x} &= \mathbf{A}x + \mathbf{B}u \\ y &= \mathbf{C}x \end{aligned} \tag{1}$$

where $\mathbf{A}$, $\mathbf{B}$ and $\mathbf{C}$ are matrices, u is the input and y is the measurement. Suppose that q failure modes, associated with actuator, plant, and sensor faults, occur in the system. Then, for the purposes of fault-detection filter design [15] the system equations in the presence of a fault have the uniform structure

$$\begin{aligned} \dot{x} &= \mathbf{A}x + \mathbf{B}u + \sum_{i=1}^{q} F_i \mu_i \\ y &= \mathbf{C}x \end{aligned} \tag{2}$$

where F_i are assumed known fault direction vectors related to each fault and μ_i (failure magnitudes) are unknown arbitrary time functions. We assume that F_i are monic, so that $\mu_i \neq 0$ implies that $F_i\ \mu_i \neq 0$. Equation (2) represents the physical way plant and actuator faults enter a system. To include sensor faults in this form requires a transformation [15].

The detection filter is a linear observer

$$\dot{\hat{x}} = \mathbf{A}\hat{x} + \mathbf{B}u + \mathbf{L}(y - \mathbf{C}\hat{x}) \tag{3}$$

where the gain $\mathbf{L}$ is to be chosen so that the residual associated with a particular fault has a unique directional behavior. Define a residual, r, between the true measurement, y, and the estimate measurement $\hat{x}$ such that

$$r = (y - \mathbf{C}\hat{x}) \tag{4}$$

Subsequently, by defining the error between true state, (x), and estimated state, $(\hat{x})$, $e = (x - \hat{x})$, from equations (2), (3) and (4), the error system dynamic equation is obtained as

$$\begin{aligned} \dot{e} &= (\mathbf{A} - \mathbf{LC})\, e + \sum_{i=1}^{q} F_i \mu_i \\ r &= \mathbf{C}e \end{aligned} \tag{5}$$

If the observer gains $\mathbf{L}$ are chosen such that $(\mathbf{A}\text{-}\mathbf{LC})$ is stable and if $(\mathbf{C}, \mathbf{A})$ is observable, then after a transient response and in absence of disturbances, the steady state residual r is nonzero only if μ_i are different from zero. Therefore, any stable observer can detect the fault by monitoring the residual. A more difficult task is to determine which of the q faults has occurred. The fault detection filter is capable of distinguishing among them. The idea is to define the filter gains $\mathbf{L}$ such that the error e remains in an invariant subspace when the fault occurs. This invariant subspace is called a detection space. These subspaces must not overlap each other in order to guarantee the identification of the fault. The invariance of the subspaces with the condition given as follows, implies that the residual r has fixed directions. In order to isolate the faults, projectors H_i are designed such that the projected residual $(R_i = H_i r)$ is sensitive only to the i-th fault. There are several algorithms developed

for determining the filter gains. In our analysis, the algorithm adopted is from Douglas and Speyer, reference [7].

Some requirements for the fault decomposition, equation (5) must be accomplished in order to uniquely identify the fault and are:

1. *The fault vectors F_i must be output separable, i.e.* $[CF_1, \ldots, CF_q]$ *has full rank* q.

2. *The fault vectors F_i must be mutually detectable (see reference [7]).*

3. *(C, A,F_i) do not have invariant zeros at origin.*

The first requirement guarantees that each fault can be isolated from other faults. When a fault μ_i occurs, the error e remains in a fixed subspace and the residual remains in an associated output subspace. If all the output subspaces are independent, the fault can be identified by projecting the residual. The second requirement, ensures that the filter eigenvalues can be assigned arbitrarily. To arbitrarily assign all eigenvalues of $A - LC$ requires that the sum of the ranks of all the detection spaces be equal to the rank of the detection space constructed from all the faults combined together. The third requirement guarantees that the projected residuals are non zero in steady state as long as their associated faults exists. All the mathematical issues and details relate to the design as well as the filter limitations, are extensively described in reference [7].

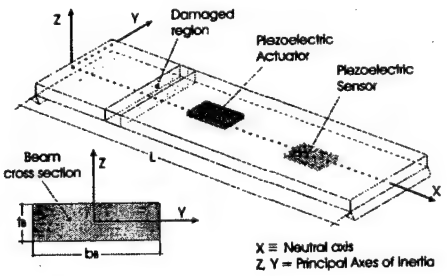

Figure 1: Scheme of the simply supported beam. Included are the damaged region, one piezoelectric sensor and one piezoelectric actuator

3 Simply supported beam

The structure is an aluminum simply supported beam of rectangular cross section with a piezoelectric actuator placed on the bottom of the beam surface and piezoelectric sensors placed on the beam top surface, as shown in figure (1). The reference frame is taken from the center of the cross section such that the x-axis coincides with the beam neutral axis. The analysis is limited to the bending behavior of the structure and small deformations are assumed. The Euler-Bernouilli hypothesis are assumed of plane sections that rotate because of bending and remain plane after deformation [16]. The beam's potential (P_B) and kinetic energy (T_B) is expressed in terms of vertical displacements, $w(x,t)$, [16]

$$P_B = \frac{1}{2}\int_{V_B} E_B\left\{-z\frac{\partial^2 w}{\partial x^2}\right\}^2 dV, \quad T_B = \frac{1}{2}\int_{V_B} \rho_B\left\{\left(\frac{\partial w}{\partial t}\right)^2 + z^2\left(\frac{\partial^2 w}{\partial x \partial t}\right)^2\right\}dV \qquad (6)$$

where E_B and ρ_B are the structure Young's Modulus and mass density, respectively and the integrals are extended to the beam volume V_B. Equation (6) is valid only for an undamaged structure. However, when damage is present, different expressions are necessary. In order to represent a crack-type damage, a region of the structure is modelled such that the crack-type damage has different stiffness (Young's Modulus) when compared with the undamaged structure (see figure 1). The mass density of damaged region is assumed unchanged because of the negligible mass reduction due to a crack. The displacements across the undamaged-damaged-undamaged interfaces are assumed continuous. With these assumptions, the kinetic energy, T_B, remains unchanged while the volume integral of the potential energy must be partitioned because the Young's Modulus is not constant along the structure length. By defining V_{BD} and E_{VB} the volume and Young's Modulus of the damaged region, respectively, the potential energy for the damaged structure can be written as:

$$P_{BD} = \frac{1}{2}\int_{V_B} E_B\left\{-z\frac{\partial^2 w}{\partial x^2}\right\}^2 dV + (E_{BD} - E_B)\int_{V_{BD}}\left\{-z\frac{\partial^2 w}{\partial x^2}\right\}^2 dV \qquad (7)$$

For the piezoelectric actuator, the potential energy must account for the electro-mechanical coupling and this can be done by introducing the electrical enthalpy, [17]

$$P_A \equiv G = \frac{1}{2}\int_{V_A}\left\{E^E\left(-z\frac{\partial^2 w}{\partial x^2}\right)^2 - 2\, d_{31}E^E\left(-z\frac{\partial^2 w}{\partial x^2}\right)\widetilde{E} - \epsilon^\varepsilon \widetilde{E}^2\right\}dV \qquad (8)$$

where V_A is the actuator volume, E^E is the actuator Young's Modulus obtained at constant electric field, d_{31} is the piezoelectric stress/charge coefficient, $\widetilde{E}$ is the applied electric field and ϵ^ε is the transducer permittivity assumed constant. Equation (8) is obtained in the hypothesis of piezoelectric transducer polarized in the thickness direction and considering its longitudinal deformations as the only relevant for the case. Note that, the first term of equation (8), represents the potential energy due to the strain energy while the remaining two terms are the contribution of the electric field.

Equation (8) could be utilized for the sensor as well. However, for the sensor, given the small electric field experienced, the strain energy contribution to the overall energy is predominant and the electrical terms can be neglected. Thus, the potential energy for the sensor can be written as

$$P_S = \frac{1}{2}\int_{V_S}\left\{E_S\left(-z\frac{\partial^2 w}{\partial x^2}\right)^2\right\}dV \tag{9}$$

where V_S is the sensor volume and E_S is the sensor Young's Modulus.
The kinetic energy for the actuator, T_A and sensor, T_S, are: [16]

$$\begin{aligned} T_A &= \frac{1}{2}\int_{V_A}\rho_A\left\{\left(\frac{\partial w}{\partial t}\right)^2 + z^2\left(\frac{\partial^2 w}{\partial x \partial t}\right)^2\right\}dV \\ T_S &= \frac{1}{2}\int_{V_S}\rho_S\left\{\left(\frac{\partial w}{\partial t}\right)^2 + z^2\left(\frac{\partial^2 w}{\partial x \partial t}\right)^2\right\}dV \end{aligned} \tag{10}$$

where ρ_A and ρ_S are the actuator and sensor mass density, respectively.

The equation of motion are obtained by applying the Rayleigh-Ritz method, [16], that approximates the unknown displacements $w(x,t)$ with a series of shape functions referred to as *admissible functions*. These functions are required to satisfy the natural boundary condition that for the simply supported beam are $w(0,t) = w(L,t) = 0$. For this case sinusoidal functions are eligible as shape functions and the displacement $w(x,t)$ are expressed as

$$w(x,t) = \sum_{j=1}^{q} B_j(t)\ \sin\left(\frac{j\pi x}{L}\right) = \sum_{j=1}^{q} B_j(t)\ \sin(k_j x) \tag{11}$$

Note that these admissible functions coincide with the mode shapes of the structure and therefore provide us with some physical information of the dynamic behavior of the beam. Upon substitution of equation (11) into equations (7)- (10), the potential and kinetic energy

are expressed in terms of the series expansion coefficients $B_j(t)$. The system *Lagrangian*, $\mathcal{L}\big(B_j(t), \dot{B}_j(t), t\big) = T_{Tot} - P_{Tot}$, is thereby obtained by collecting the energy expressions of the sensor, actuator and beam. By means of *Lagrange's Equations*, the *Lagrangian* provides the equation of motion

$$[M]\{\ddot{X}(t)\} + [K]\{X(t)\} = \{Q\} \tag{12}$$

where $\{X(t)\} = \{B_1,\ B_2,\ \ldots,\ B_q\}^T$ is the generalized vector, $[M]$ and $[K]$ are the generalized mass and stiffness matrices, respectively and $\{Q\}$ is the generalized forcing terms. In the equation of motion, damping is included by means of modal coefficients, ξ_j, whose values are evaluated based on the experimental measurements, [18]

$$[D] = [M]\ \Phi\ \Lambda\ \Phi^T\ [M], \quad \Lambda = \begin{bmatrix} \ddots & & \\ & 2\ \xi_j\ \omega_j & \\ & & \ddots \end{bmatrix} \tag{13}$$

In equation (13), ω_j are the system natural frequencies and the matrix Φ is obtained with the system eigenvectors ordered column-wise $\Phi = [\phi_1,\ \phi_2,\ \ldots, \phi_n]$. By means of equation (13), the equation of motion can be written in its final form

$$[M]\{\ddot{X}(t)\} + [D]\{\dot{X}(t)\} + [K]\{X(t)\} = \{Q\} \tag{14}$$

3.1 State-variable description

The equation of motion (14), is rearranged in a linear time invariant state space form

$$\begin{aligned} \dot{\zeta}(t) &= \mathbf{A}\zeta(t) + \mathbf{B}\Delta\phi_A \\ X(t) &= \mathbf{C}^*\zeta(t) \end{aligned} \tag{15}$$

where the state vector is defined by means of the generalized displacement vector $\zeta(t) = \{X(t)\ ,\ \dot{X}(t)\}^T$, $\Delta\phi_A$ is the voltage input applied to the actuator and $\mathbf{A}$, $\mathbf{B}$ and $\mathbf{C}^*$ are

defined as follows[1]

$$\mathbf{A} = \begin{bmatrix} \mathbf{0} & \mathbf{I} \\ -M^{-1}K & -M^{-1}D \end{bmatrix}, \quad \mathbf{C}^* = [\mathbf{I}\ ,\ \mathbf{0}]$$
$$\mathbf{B} = \begin{Bmatrix} \mathbf{0} \\ Q^* \end{Bmatrix}, \qquad Q^* \Delta\Phi_A = Q \tag{16}$$

The output from equation (15) is the generalized displacement vector, whose components are the coefficients of the series expansion, equation (11).

For the current analysis, the output voltage from each sensor is required which is proportional to the strains experienced by the piezoelectric. Because this voltage is generally very small, the hypothesis of *zero flux*, [17], can be issued such that, neglecting the transversal deformation, gives

$$\tilde{E}_i(x,z,t) = -\, d_{31}\, \frac{E_S^E}{\epsilon^{SL}} \left(-z \frac{\partial^2 w}{\partial x^2} \right)_{x \equiv x_i} \tag{17}$$

In equation (17), in addition to the quantities defined in equation (8), the parameter ϵ^{SL} is utilized which represent the *clamped* piezoelectric permittivity [17]. The voltage output is obtained as the averaged value along the sensor electrodes of the integral of the electric field over its thickness, i.e.

$$\Delta\phi_{Si} = \alpha \int_{x_{1Si}}^{x_{2Si}} \int_{t_B/2}^{t_B/2+t_{Si}} \left(-z \frac{\partial^2 w}{\partial x^2} \right) dz\, dx$$
$$\alpha = -\, d_{31}\, \frac{E_S^E}{\epsilon^{SL}} \frac{b_{Si}}{|x_{2Si} - x_{1Si}|} \tag{18}$$

where b_{Si} is the sensor width, t_{Si} is the sensor thickness and x_{1Si}, andx_{2Si}, are the starting and ending abscissaes of the sensor. This integration processes can be included in the state variable form by defining a new matrix $\mathbf{C}$ as follows

$$[\mathbf{C}] = \begin{bmatrix} \beta_1 \\ \beta_2 \\ \vdots \\ \beta_4 \end{bmatrix} [\mathbf{C}^*] \quad \longrightarrow \quad \mathbf{\Delta\phi_S} = \begin{Bmatrix} \Delta\phi_{S1}(t) \\ \Delta\phi_{S2}(t) \\ \vdots \\ \Delta\phi_{Sn}(t) \end{Bmatrix} = [\mathbf{C}]\zeta(t) \tag{19}$$

[1]In order to reduce the symbology, the following notation is adopted: $[M] \equiv M$, $[K] \equiv K$ and $[Q] \equiv Q$.

where $\Delta\phi_{Si}$ are the voltage outputs of each sensor and the vectors β_i are obtained after integration of equation (18). The final form of the state variable description can be written as

$$\begin{aligned} \dot{\zeta}(t) &= \mathbf{A}\zeta(t) + \mathbf{B}\Delta\phi_A \\ \mathbf{\Delta\phi_S} &= \mathbf{C}\zeta(t) \end{aligned} \tag{20}$$

For the simply supported beam described in this paper, the number of mode-shapes employed in equation (11) is 14 and therefore stiffness, mass and damping matrices have dimensions: $dim(M) = dim(K) = dim(D) = 14 \times 14$, respectively, while the matrix $\mathbf{A}$ has dimension $dim(\mathbf{A} = 28 \times 28)$. One actuator and four sensors where utilized so that the resulting $\mathbf{B}$ and $\mathbf{C}$ matrices have dimensions $dim(\mathbf{B}) = 28 \times 1$ and $dim(\mathbf{C}) = 4 \times 28$, respectively.

3.2 Fault decomposition

In order to utilize the fault detection filter, the structural damage needs to be reduced to the form in equation (2), which implies the generation of the fault direction vectors, F_i and the failure amplitudes, μ_i. This can be achieved as follows. By assuming that a fault occurs in the beam, and no faults occurs in the sensor and actuator arrays, the $\mathbf{A}$ matrix (equation (16)), changes as follows

$$\overline{\mathbf{A}} = (\mathbf{A} + \delta\mathbf{A}) = \begin{bmatrix} 0 & I \\ M^{-1}K & M^{-1}D \end{bmatrix} + \begin{bmatrix} 0 & 0 \\ M^{-1}\delta K & 0 \end{bmatrix} \tag{21}$$

where δK is the variation of the stiffness matrix. Recall that it is assumed that the damage effects only the stiffness of the structure while its mass remains unmodified.

The matrix $\delta\mathbf{A}$ can be decomposed by means of a singular value decomposition. Note that, from equation (21), the rank of the matrix $\delta\mathbf{A}$ is essentially related to the rank of the matrix δK and therefore, the singular value decomposition of δK is

$$\delta K = U\ \Sigma\ V \tag{22}$$

By defining the *fault direction matrix*, F, and *failure amplitude*, μ, as follow

$$F = \begin{Bmatrix} 0 \\ M^{-1}U \end{Bmatrix}, \quad \mu = \begin{Bmatrix} 0 & \Sigma V \end{Bmatrix} \zeta \tag{23}$$

with Σ and ζ, the state vector, being unknown, the state variable description of the damaged structure can be written as:

$$\begin{aligned} \dot{\zeta}(t) &= \mathbf{A}\zeta(t) + \mathbf{B}\Delta\phi_A + F\,\mu \\ \Delta\phi_S &= \mathbf{C}\zeta(t) \end{aligned} \tag{24}$$

This procedure can be repeated for each fault location. For the structure in consideration, recalling that a total of 14 mode shapes or shape functions were utilized, the resulting state dimension was $\mathbb{R}^{28}$. The matrix δK was obtained for numerous fault locations and for different damage sizes. However, it was noticed that, when the fault size was sufficiently small, the rank of the δK matrix was constant ($rank(\delta K) = 1$) for all the different positions simulated. Therefore, 1 fault direction vector, F_i, ($dim(F) = 28 \times 1$) and 1 failure amplitude, μ_i, ($dim(\mu) = 1 \times 1$) is associated with each of the infinite fault positions. This can be seen in figure (2) where the first two singular values of the δK matrix obtained at a fixed damage position and for different damage sizes are shown. The damage sizes are expressed as percentage of the beam length. It can be seen from figure (2) that, while the magnitude of one singular value is approximately constant, the magnitude of other drops sharply with the decrease of fault size. Therefore, because we were interested in detecting damage at the earliest stage possible, that is for a fault magnitude as small as possible, only the vector associated with the greatest singular value was kept as fault direction vector for our analysis.

In addition to the rank of the δK matrix, the variation in *directions* of the fault vectors was investigated as function of the damage size. A baseline fault direction vector was obtained by simulating a damage in a generic position whose size was 1% of the beam length. Then, the damage size was varied and the new resulting fault detection vector was compared with the baseline. The comparison was obtained by means of the inner product between the two vectors and the results are shown in figure (3). From the figure, it can be seen that, up to approximately 4% size, the inner product is close to unity, meaning that

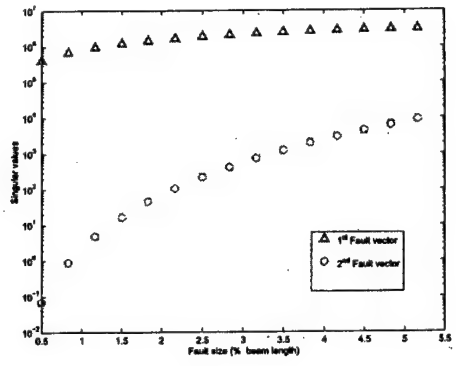

Figure 2: Singular values relative to the 4 vectors obtained from the decomposition of the simply supported beam, obtained for different fault sizes.

the directions of these vectors do not change significantly.

Based on these two investigations, we concluded that any sufficiently small damage sizes produces only one significant fault direction vector, whose amplitude and direction is approximately *independent* of fault size, and only *dependent* on fault location. Therefore, for each of the infinite damage locations, one can associate one fault vector and a fault detection filter can be used to detect and locate each of them. More detail of this fault decomposition can be found in reference [19].

4 Filter Design

The filter design is implemented by defining pre-simulated fault locations forming a basis for the identification of each of the infinite possible faults that might occur. The algorithm is obtained from reference [7] and adapted to the beam structure. For this case, based on the Douglas-Speyer theory to build only *one* detection filter requires that as many measurements as half of the dimension of the state vector be available. For example, because $\mathbb{R}^{28}$, the number of measurements required would be $n=14$. However, requiring this many sensors can be a limiting issue for practical implementations and a modification of the original algorithm is presented here. The algorithm is implemented by designing five filters, each

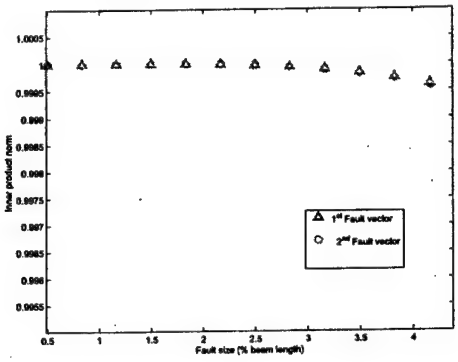

Figure 3: Inner product of fault vectors when the fault size is varied maintaining fixed the fault position.

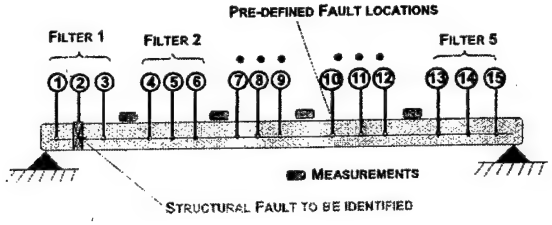

Figure 4: Scheme of the simply supported beam with 4 measurements and 15 simulated faults used in the design of 5 fault detection filters.

of them utilizing three pre-defined fault direction vectors positioned evenly in the interval between two sensors. A scheme of the measurements and the pre-defined fault locations is shown in figure (4). Although the algorithm is presented for this specific case of four sensors, $s = 4$, it can be adapted for virtually any number sensors providing $s \geq 2$.

The pre-defined fault direction vectors satisfies the three requirements listed in section(2), i.e. are mutually detectable, output separable, and ($\mathbf{C}$,$\mathbf{A}$, F_i) do not have invariant zeros at origin. For each filter design one wants to choose the filter gains, $\mathbf{L}$, such that, if a fault occurs, the residual remains in an invariant subspace τ_i (detection space). To ensure this, the filter eigenvalues are assigned such that they have equal values. In order to uniquely identify each fault, these subspaces need to be non intersecting with each other, and their dimension must entirely fill the system space. The detection spaces associated with each

fault, τ_i, have dimension $dim(\tau_i) = 2$. Therefore, the three detection spaces do not fill the dimension of the state space. For example, for filter one, the detection spaces associated with the faults F_1, F_2 and F_3 (see figure (4)), are τ_1, τ_2 τ_3, and

$$\tau_1 \cup \tau_2 \cup \tau_3 = \mathbb{R}^6 \tag{25}$$

and the resulting complementary subspace has dimension $\mathbb{R}^{22}$. The detection space is obtained by assigning 2 equal eigenvalues for all the 3 fault direction filters. The complementary space is instead obtained by assigning additional 22 eigenvalues. In this design procedure, the sets of eigenvalues chosen were complex conjugated and equal for each filter, although this is not a requirement, it allows fault directions at arbitrary damage locations to appear in invariant directions in residual space. The procedure for establishing the detection spaces and the complementary space follows next and is described separately.

4.1 Detection space

As previously mentioned, 5 filters are designed for the simply supported beam scenario and each filter relays on 3 pre-defined fault locations. We use 3 pre-defined fault locations rather than 4, because with 4 the system is not mutually detectable and therefore, all the filter eigenvalues can not be chosen arbitrarily. The procedure here described is the same for each filter. From reference [7], the filter gains, $\mathbf{L}$, can be obtained by left-eigenvector assignment as follows:

$$\begin{bmatrix} \lambda_i I - \mathbf{A}^T & \mathbf{C}^T \\ \hat{F}_p{}^T & 0 \end{bmatrix} \begin{Bmatrix} V \\ W \end{Bmatrix} = \begin{bmatrix} 0 \\ 0 \end{bmatrix}, \quad p = 1, 2, 3 \tag{26}$$

where the matrix $\hat{F}_p$ is obtained collecting column-wise all the fault direction vectors except the p-th. As previously mentioned, the two eigenvalues used in this algorithm are of complex conjugate, i.e. $\lambda_i \rightarrow \lambda$ and λ^*. By means of equation 16, the above equation (26) can be

rewritten in its partitioned form,

$$\begin{bmatrix} \lambda_i I & -(A_a)^T & C_0^T \\ -I & \lambda_i I + (A_b)^T & 0 \\ 0 & (\hat{F}_b^T)_p & 0 \end{bmatrix} \begin{Bmatrix} V_1 \\ V_2 \\ W \end{Bmatrix} = \begin{Bmatrix} 0 \\ 0 \\ 0 \end{Bmatrix} \tag{27}$$

$$A_a = (M^{-1}K), \quad A_b = (M^{-1}D)$$

where the matrices $\hat{F}_b^T$ [2] and C_0 [3] are obtained from equation (19) and (22), respectively. The dimensions of the left matrix of equation (26) are 30×32 and its range space has dimension 30. Although its resulting null space is two-dimensional, in the algorithm presented here, only one of the two null vectors is employed. From the third row of equation (27), because $dim((\hat{F}_b^T)_p) = 2 \times 14$ and its rank is $rank((\hat{F}_b^T)_p) = 2$, we obtain 12 independent vectors V_2 that span its null space

$$(\hat{F}_b^T)_p V_2 = 0 \;\rightarrow\; (V_{2k})_p^i, \quad k = 1, 2, \ldots, 12. \tag{28}$$

By substituting these twelve vectors into the second row of equation (27), a total of 12 (complex) vectors V_1 are obtained

$$\begin{aligned} &(V_{1k})_p^i = (\lambda_i I + A_b)(V_{2k})_p^i = (V_{1k}^R)_p^i + j(V_{1k}^I)_p^i \\ &\qquad\qquad \text{where :} \\ &(V_{1k}^R)_p^i = (a_i I + A_b)(V_{2k})_p^i \\ &(V_{1k}^I)_p^i = (b_i I + A_b)(V_{2k})_p^i. \end{aligned} \tag{29}$$

By substituting a linear combination of the twelve vectors, V_1 and V_2, in the first row of equation (26)

$$\lambda_i V_1 + A_a V_2 + C_0^T W = 0 \tag{30}$$

---

[2] From equation (22), the generic fault direction vector, is defined as $F_i = \left\{0 \ , \ (M^{-1}U_i)^T\right\}^T$ and can be rewritten as $F_i = \left\{0 \ , \ F_b^T\right\}^T, \quad dim(F_b) = 14 \times 1$

[3] From equation (19), the matrix **C** can be rewritten as

$$[\mathbf{C}] = \begin{bmatrix} \beta_1 \\ \vdots \\ \beta_4 \end{bmatrix} [\mathbf{I} \ , \ \mathbf{0}] = [C_0 \ 0]$$

and $dim(C_0) = 14 \times 14$

and by defining α_k^i, the generic coefficients of their linear combination, after rearranging the terms, one obtains

$$\left[(M_1)_p^i \ldots\ (M_{12})_p^i,\ (C_0^T)_1,\ (C_0^T)_2\right] \begin{Bmatrix} \alpha_1^i \\ \alpha_2^i \\ \vdots \\ \alpha_{12}^i \\ w_1 \\ w2 \end{Bmatrix} = -\left[(C_0^T)_3,\ (C_0^T)_4\right] \begin{Bmatrix} w_3 \\ w_4 \end{Bmatrix} \tag{31}$$

In the above equation, w_1, w_2, w_3 and w_4 are the unknown components of the vector W, $(C_0^T)_s$, $s = 1, 2, 3, 4$ are the column components of the matrix C_0^T and the complex vectors $(M_k)_p^i$ are

$$\begin{aligned} (M_k)_p^i = \left\{(M_k^R)_p^i + j(M_k^I)_p^i\right\} = \left\{a_i(V_{1k}^R)_p^i - b_i(V_{1k}^I)_p^i\right. \\ \left. + A_a(V_{2k})_p^i\right\} + j\left\{b_i(V_{1k}^R)_p^i + a_i(V_{1k}^I)_p^i\right\} \end{aligned} \tag{32}$$

Since the vectors $(M_k)_p^i)$ and $(C_0^T)_s$ have dimensions $dim((M_k)_p^i) = dim((C_0^T)_s) = 14 \times 1$, equation (31) yields 14 algebraic equations with 16 unknown coefficients: α_k, $k = 1, 2 \ \ldots\ 12$, and w_1, w_2, w_3, w_4, respectively. Because the vectors $(M_k)_p^i)$ and $(C_0^T)_s$ are found to be linearly independent and the matrix on the left side of equation (31) has full rank, a solution is obtained by assigning arbitrarily, two values, say w_3 and w_4. After recovering the coefficients α_k^i from equation (31), they are substitute back to equation (29) to obtain the two unknown vectors $(V_1)_p^i$ and $(V_2)_p^i$ for each p-th fault and for each i-th eigenvalue.

??

$$\begin{aligned} (V_2)_p^i &= \sum_{k=1}^{12} \alpha_k^i (V_{2k})_p^i \\ (V_1)_p^i &= \sum_{k=1}^{12} \alpha_k^i (a_i I + A_b)(V_{2k})_p^i + j \sum_{k=1}^{12} \alpha_k^i (b_i I + A_b)(V_{2k})_p^i \end{aligned} \tag{33}$$

The vectors V_1, V_2, and $(W)_p^i = [w_1,\ w_2,\ w_3,\ w_4]^T$, composed together, constitute the null-space vectors solution of equation (26). The procedure is repeated for each of the p fault vectors, $p = 1, 2, 3$, and for each of the two eigenvalues λ_1 and λ_1^* chosen for the

detection spaces so that six independent vectors are obtained [4]

$$V_D = \begin{bmatrix} (V_1)_1^1 & (V_1^*)_1^1 & \dots & (V_1)_3^1 & (V_1^*)_3^1 \\ (V_2)_1^1 & (V_2^*)_1^1 & \dots & (V_2)_3^1 & (V_2^*)_3^1 \end{bmatrix}$$
$$W_D = \begin{bmatrix} (W)_1^1 & (W^*)_1^1 & \dots & (W)_3^1 & (W^*)_3^1 \end{bmatrix}. \tag{34}$$

4.2 Complementary space

The procedure to obtain the null space of the *complementary spaces* is similar to the one described for the *detection space*. As usual, the detection space basis is obtained by left-eigenvector assignment of (26) or its partitioned form

$$\begin{bmatrix} \lambda_i I & -(A_a)^T & C_0^T \\ -I & \lambda_i I + (A_b)^T & 0 \\ 0 & (\hat{F}_b^T) & 0 \end{bmatrix} \begin{Bmatrix} V_1 \\ V_2 \\ W \end{Bmatrix} = \begin{Bmatrix} 0 \\ 0 \\ 0 \end{Bmatrix} \quad i = 1, 2, \dots, 11$$
$$A_a = (M^{-1}K), \quad A_b = (M^{-1}D) \tag{35}$$

All the matrices of equation are unchanged except the matrix $(\hat{F}_b^T)$ of the 3^{rd} row that now includes all the filter fault directions. For example, for filter 1, F_b^T is

$$F_b^T \triangleq [F_1,\ F_2,\ F_3] = \begin{Bmatrix} 0 \\ F_b \end{Bmatrix}, \quad dim(F_b^T) = 3 \times 14 \tag{36}$$

As consequence, the dimension of the left matrix of equation (35) is now 31×32 and, because its range space has dimension equal to 31, the resulting null space is one-dimensional yielding a unique null vector. As usual, in order to obtain this null vector, it is convenient to solve piecewise the equation (35). From the third row of equation (35), the matrix F_b^T has $dim(F_b^T) = 3 \times 14$ and $rank(F_b^T) = 3$ yielding 11 vectors, V_2 for each eigenvalues λ_i

$$(F_b^T)V_2 = 0 \qquad \rightarrow (V_{2k})^i \equiv V_{2k},\ k = 1, 2\ \dots\ , 11. \tag{37}$$

[4] The asterisk indicates the complex conjugate vectors.

By substituting the obtained vectors $(V_{2k})^i$ in the second row of equation (35), analogously as for the previous case, 11 vectors $(V_1)^i$ are found.

The first row of equation (35) provides the vector W after substituting a linear combination of the vectors $(V_{1k})^i$ and $(V_{2k})^i$. Similarly as for the procedure adopted in the detection filter, by defining α_k^i, the generic coefficients of the linear combination, and by naming as w_1, w_2, w_3 and w_4, the unknown components of the vector W, the first row of equation (35), after rearranging the terms, becomes

$$\left[(M_1)^i, \ldots\ (M_{11})^i,\ (C_0^T)_1,\ (C_0^T)_2,\ (C_0^T)_3\right] \begin{Bmatrix} \alpha_1^i \\ \alpha_2^i \\ \vdots \\ \alpha_{11}^i \\ w_1 \\ w2 \\ w_3 \end{Bmatrix} = -\left[(C_0^T)_4\right] w_4 \tag{38}$$

where $(C_0^T)_s$, $s = 1, 2, 3, 4$ are the column component of the matrix C_0^T and the complex vectors $(M_k)^i$ are obtained in a similar way as for equation (32). Notice that equation (38) is a set of 14 algebraic equations with 15 unknowns: α_k^i, $k = 1, 2, \ldots\ 11$, and w_1, w_2, w_3 and w_4. On the other hand, the vectors $(M_k)^i$ and $(C_0^T)_s$, for this case are verified to be linearly independent and thus the left side matrix of equation (38) is invertible. A solution is therefore possible by assigning the value of one component, say w_4. Thus, equation (38) provides the coefficients α_k^i of the linear combination of vectors $(V_{1k})^i$ and $(V_{2k})^i$ and the two vectors $(V_1)^i$ and $(V_2)^i$ are recovered as

$$(V_2)^i = \sum_{k=1}^{12} \alpha_k^i V_{2k}, \quad (V_1)^i = \sum_{k=1}^{12} \alpha_k^i V_{2k} \tag{39}$$

The procedure is repeated for each of the eigenvalues λ_i and λ_i^* chosen for the complementary spaces, to obtain a total of 22 independent vectors. These vectors are ordered into

the following two matrices,

$$V_C = \begin{bmatrix} (V_1)^1 & (V_1^*)^1 & \dots & (V_1)^{11} & (V_1^*)^{11} \\ (V_2)^1 & (V_2^*)^1 & \dots & (V_2)^{11} & (V_2^*)^{11} \end{bmatrix}$$
$$W_C = \begin{bmatrix} (W)^1 & (W^*)^1 & \dots & (W)^{11} & (W^*)^{11} \end{bmatrix}. \tag{40}$$

Once the vector sets, V_1, V_2 and W are obtained for both the detection spaces and complementary space, the matrices defined in equations (34) and (40) are rearranged as follows:

$$\mathbf{V} = [V_D,\ V_C],$$
$$\mathbf{W} = [W_D,\ W_C] \tag{41}$$

and the final filter gains are obtained as

$$\mathbf{L}^T = \mathbf{W}(\mathbf{V})^{-1} \quad \text{or } \mathbf{L} = (\mathbf{V}^T)^{-1}\mathbf{W}^T \tag{42}$$

4.3 Numerical simulation and optimal design

In order to illustrate the use of the fault detection filter here proposed for health monitoring, we refer to the scheme of figure (4). As already stated, the figure shows the beam structure with 15 pre-defined fault locations utilized for the design of 5 distinct fault detection filters. For this simulation, a structural fault is also included and its position is coincident with the pre-defined fault location 2. A step input is applied to the actuator. The filter estimate is compared with the output from the sensors to create the system residuals (see equation (4)). The residuals are projected with residual projectors that annihilate all the faults except the one for which they are designed for. The resulting norm of projected residuals obtained for filter 1 and filter 3 are shown in figure (5)and figure (6), respectively. The response is shown in both time and frequency domain. As one can see from figure (5), for filter 1 that experience the structural faults, the response of the projector designed for the pre-defined fault 2 is approximately 150 dB greater than the other two. This indicates that a probable faults has occurred in the pre-defined location 2. A similar scenario is unlikely to happen for the remaining filters. As shown in figure (6), all the three norms of

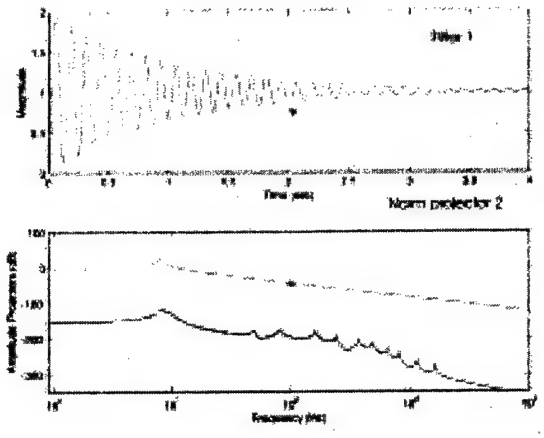

Figure 5: Time and frequency domain of the norm of the projected residuals of filter 1.

the projected residuals of filter 3, have comparable magnitude indicating that none of them has experienced a the fault for which it was designed.

The procedure of detecting and localizing the fault is here described for a structural fault that coincides with one of the pre-defined fault location. However, it can be shown that similar procedure can be applied to identify structural faults at generic locations with same filters but utilizing different projectors mapping the entire structure (see reference [19]) .

Based on the analytical simulation described, the in-situ health monitoring system should be automated by using post-processing residuals that would provide the probability that a faults has occurred in one of the five filters and also determine the fault exact location. An important aspect that should be considered is the type of input that should be utilized in real systems. In fact, the step input utilized in our simulation is difficult to reproduce with piezoelectric transducers. More realistic inputs are periodic excitations such as single sinusoidal waves and their frequencies should be chosen based on the dynamic response of the structure. The best response of the structure is in the vicinity of its natural frequencies and therefore, those would be perfect candidates and guarantee a good sensitivity to damage. For the simply supported beam described in this paper, the sinusoidal waves investigated as input for the piezoelectric actuator coincided with the first few structural natural frequencies and the filter design was optimized according to them.

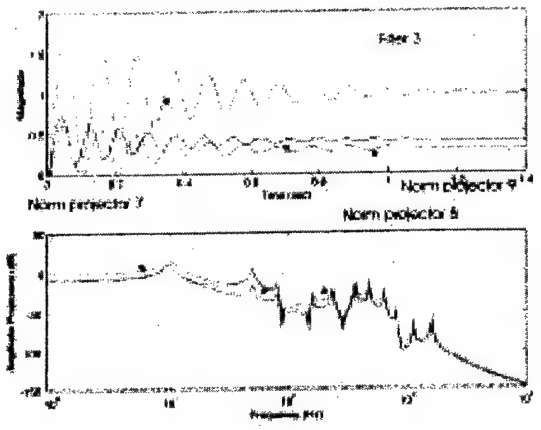

Figure 6: Time and frequency domain of the norm of the projected residuals of filter 3.

In order to have satisfactory sensitivity to damage, in addition to using an optimal input, the filter gains were also investigated. An important aspect that was considered was the rejection of disturbances and noise. According to the scheme of figure (7), the transmission noise, n, to residuals, r, can be written as

$$\frac{n}{r} = \mathbf{H}\{I - \mathbf{C}\,[sI - (\mathbf{A\text{-}LC})]^{-1}\,\mathbf{L}\} \tag{43}$$

and it can be seen that it can be reduced by reducing the filter gains, L. A typical trans-

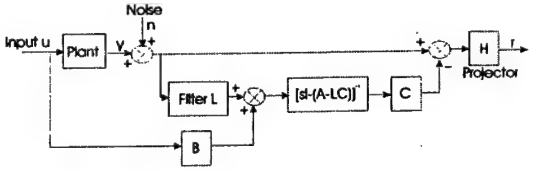

Figure 7: Scheme of the transmission noise, n, to residual, r.

mission obtained in our optimal design is shown in figure (8) and is relative to filter N^o 5. As it can be seen from the figure, considering that the inputs used for this structure are in the low frequency range, the noise transmission amplitude is kept low up to approximately 100 Hz, where are the first 3 natural frequency. Notice, however, that in the high frequency range, the noise transmission amplitude is considerably high in the order of 100 dB and therefore, the system inputs and outputs required band-pass filters to avoid this high fre-

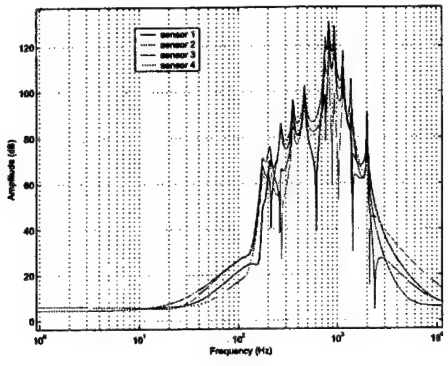

Figure 8: Transmission noise to residual for filter N^o 5

Filter N^o	Fault N^o
Filter 1	3, 8, 11
Filter 2	13, 15, 9
Filter 3	2, 5, 10
Filter 4	1, 6, 14
Filter 5	4, 7, 12

Table 1: Optimally clustered pre-defined fault direction vectors

quency region. Different designs can be achieved choosing accurately the filter eigenvalues accordingly with the input used.

Another important aspect investigated is the clustering of the pre-definite damage positions into the 5 filters. In fact, the ability of each filter to distinguish among the fault direction vectors is related to the directions of such vectors. Therefore, by clustering the three pre-defined fault locations utilized for each filter such that their directions are optimally different, the sensitivity to damage can be increased. The optimal configuration obtained for the current setup is represented in table (1).

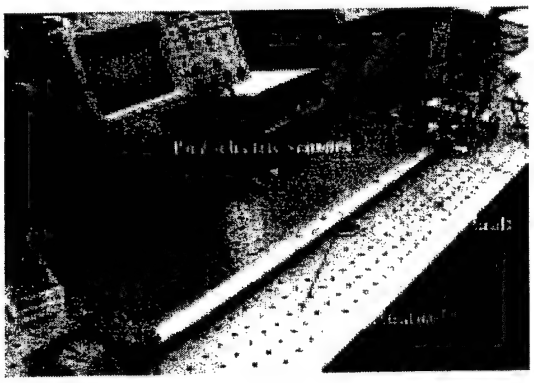

Figure 9: Experimental test setup.

5 Results and Discussions

The experimental setup of the aluminum simply supported beam is shown in figure (9) and the material properties and dimensions used in the analytical model are listed in table (2). The piezoelectric sensors are positioned on top of beam surface along the longitudinal

	Beam	Sensor and Actuator
Thickness	t_B 3.2 mm	$t_S =$ 0.125 mm, $t_A = 0.6$ mm
Width	$b_B =$ 27.5 mm	$b_S \equiv b_A =$ 2.5 mm
Length	$L =$ 0.771 m	$L_S \equiv L_A = 4$ mm
Young' modulus	$E_B = 68.9$ GPa	$E_S = 40.0$ GPa, $E_A = 80.0$ GPa
Density	$\rho_B = 2730$ kg/m^3	$\rho_S \equiv rho_A = 7750$ kg/m^3
Piezoelectric stress/charge coefficient		$d_{31} = -274 \cdot 10^{-12}$ C/N
Clamped piezoelectric permittivity		$\epsilon^{SL} =$ 2.46310^{-8} C/Nm^2

Table 2: Dimension and material properties

midline at 180 mm, 333 mm, 486 mm and 639 mm, respectively, from the left-hand edge of the beam and the piezoelectric actuator is positioned on the bottom surface, along the beam midline, at 397 mm from the left-hand edge of the beam. The position of sensors and actuator was decided based on simulation so that both observability and controllability of resulting state-space system was guaranteed. The measured frequency response of the

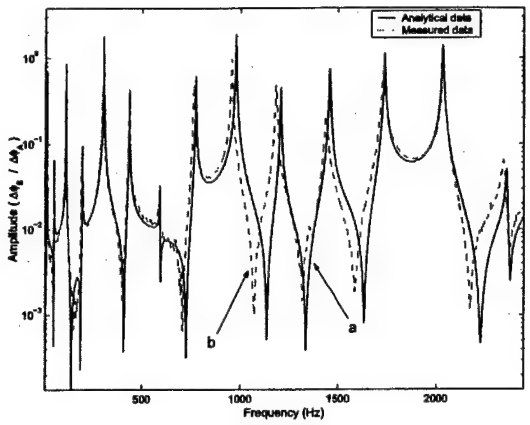

Figure 10: Input-output frequency response from actuator and sensor 1 of the simply supported beam. a) Analytical vs. b) measured data.

structure from sensor 1 is shown in In figure (10) and is compared with the analytical transfer function obtained from the model. The range of frequency shown in the figure includes the first 14 natural frequencies. The transfer function is obtained with a Stanford Research System Spectrum Analyzer, Model SR785 with 2048 points. As it can be seen from figure (10), the model provides a very good agreement with the measured data with errors in the peak frequencies approximately of the order of 2%.

For the implementation of the fault detection filter, the following equipments where utilized: 1) A Wavetek 10MHz DDs Mod. 29 function generator to produce the sinusoidal inputs for the actuator, 2) a low impedance Burleigh PZ 150M volt amplifier for the amplification of the actuator input, and 3) a National Instruments PCI-MIO-16E-1 PC card for data acquisition. The data from the sensors and actuator were sampled at 40 Ksample/sec and each acquisition lasted asted 10 seconds. In order to reduce the noise effect, digital Chebychev low pass and band-pass filter where appropriately designed for each of the input and output signals. The state integration was obtained with a Runge-Kutta fourth order method using Matlab software. The actuator input was approximately 120 Volts after amplification and the average output from the sensors was approximately 2 Volts[5]. The

[5]The average measured capacitance of each sensor is $C \cong 3nF$ resulting in high impedance and thereby high voltage output even with small currents generally experienced with piezoelectric transducers.

norms of the projected residuals obtained from the undamaged structure had magnitude of approximately 10^{-2}, indicating good tracking of the filter.

The damage inflicted upon the structure was a saw cut of approximately 5mm $\times$ 1 mm made on one side of the beam at approximately 448 mm from the beam left-hand edge. The saw cut position was chosen coincident with the pre-defined fault location N^o 9. A new set of data was taken from the damaged structure and compared with the estimate of the fault detection filter. The resulting norms of the projected residuals are shown in figure (11) for filter N^o 1 and filter N^o 4, respectively. Recall that, for this scenario, filter N^o 1 is the filter that supposedly should detect the damage. In the figure, for each filter, in case A) are shown the normalized norms of residuals before damage occurs and in case B) are shown the normalized norms of residuals after damage has occurred. The residuals are normalized with respect to values obtained before damage had occurred. As it can be seen from figure (11), in both filters, when there was no damage, all the three residuals have similar values. After damage occurred, in filter N^o 1, the norm of the pre-defined fault direction, location 9, increased approximately 3 times while the other two norms, location 13 and 15, were essentially unchanged. This indicated that the projector 9 detected a damage coincident with the fault location 9. For filter N^o 4, instead, all the residual norms increased indicating that no specific fault was detected. Although not shown, the residual norms of filter N^o 2, 3 and 5, after damage had occurred, showed a behavior similar to the one of filter N^o 4 indicating that no specific fault was detected.

Based on the previous results, one can conclude that the structure experienced damage and that the damage was probably coincident with the pre-defined fault location 9. However, for an in-situ health monitoring system, the procedure should be automated perhaps implementing post-processing residuals so that a decision can be made about the structure health [20]. Nominally, the residual is zero in the absence of a fault and nonzero otherwise. However, as previously stated, when driven by uncertainties and disturbances, the residual fails to go to zero even in the absence of faults. To enhance detection and identification, the residual processor analyzes the residual generated by the fault detection filter which can be viewed as a static geometric pattern containing information about the presence or absence

of a fault. By considering the residual processor design as a static geometric pattern recognition problem, the residual processor could be a neural network or a multiple hypothesis Shiryayev sequential probability test which detects and identifies a fault in minimum time with a given probability of false and miss alarm [20]. The fault identification problem is now solved by assuming that each fault corresponds to certain hypothesis. The residual is considered to be the measurement sequence for the multiple hypothesis Shiryayev sequential probability test which is assumed to be a given distribution (not necessarily Gaussian) and conditionally independent. The conditional probability of each fault hypothesis is generated to be used to announce the occurrence of the fault with a threshold based on a given probability of false and missed alarms. Therefore, the essential feature of the residual processor is to analyze the residue and identify a fault, if it has occurred, with an associated probability. This allows for higher level decision making which now can be based on the probability. In the development of a health monitoring system, the fault detection filter and residual processor should be designed together.

References

[1] Doebling S.W., Farrar C.R., and Prime M.B., "**Damage identification and health monitoring of structural and mechanical systems from changes in their vibration characteristics : a literature review** , Los Alamos, N.M. : Los Alamos National Laboratory, **1996**.

[2] Parloo E., Verboven P., Guillaume P., Van Overmeire M., "**Autonomous structural health monitoring. II. Vibration-based in-operation damage assessment**," *Mechanical Systems & Signal Processing*, vol.**16**, no.**4**, July **2002**, pp.659-75.

[3] Beard R.V., "**Failure Accomodation in Linear System through Self-Reorganization**," Ph.D. thesis, Massachussets Institute of Technology, **1971**.

[4] Jones H.L., "**Failure Detection in Linear Systems**," Ph.D. thesis, Massachussets Institute of Technology, **1973**.

[5] Massoumnia M-A., "**A geometric approach to the synthesis of failur filters,**" *IEEE Transactions on Automatic Contol*, vol. **AC-31**, no. **9**, pp.8 **1986**.

[6] White J.E., and Speyer J.L., "**Detection filter design: Spectral the gorithms,**" *IEEE Transactions on Automatic Control*, vol. **AC-32**, no. **7** p.593-603.

[7] Douglas R.K., and Speyer J.L., "**Robust Fault Detection Filter De:** *Journal of Guidance, control and Dynamics*, vol. **19**, No. **1**, pp. 214-218, J:

[8] Douglas R.K., and Speyer J.L., "H_∞ **Bounded Fault Detection Filter,**" *nal of Guidance, control and Dynamics*, vol. **22**, No. **1**, pp. 129-138, Jan-I

[9] Chen R.H., Ng H.K., Speyer J.L., Mingori D.L., "**Fault detection, identi: reconstruction for ground vehicles,**" *ITSC 2001. 2001 IEEE Intelligen tion Systems*, Proceedings (Cat. No.01TH8585). IEEE. **2001**, pp.924-9. Pis USA.

[10] Rajamani C., Chen A., Howell J.K., Hedrick and M. Tomizuka, " **A Com Diagnostic System for Automated Vehicles** ," *R. IEEE Transactior Systems Technology*, Vol. **9**, No. **4**, pp. 553-64, July **2001**.

[11] Laurence H.M. and Speyer J.L., "**Fault-Tolerant GPS/INS Navigat with Application to Unmanned Aerial Vehicle,**" *Journal of the Inst: gation*, vol. **49**, No. **1**, Spring **2002**.

[12] Mehra, R.K. and Peshon, I., "**An innovations approach to fault de diagnosis in dynamic systems,**" *Automatica*, Vol.**7**, pp.637-640, **1971**.

[13] Waller, H. and Schmidt, R., "**The application of state observers ir dynamics,**" *Mechanical Systems and Signal Processing*, Vol.**4**, No.3, pp.1

[14] Fritzen, C.P. and Mengelkamp, G., "**A Kalman filter approach to the detection of structural damage**," *Proceeding of the* 4^{th} *International Workshop on Structural Health Monitoring*, Stanford, CA pp.1275-1284, **2003**.

[15] Chung, W. H. and Speyer, J. L., "**A Game Theoretic Fault Detection Filter**," *IEEE Transactions on Automatic Control*, Vol.**AC-43**, No.2, pp.143-161, **1998**.

[16] Géradin M., and Rixen D., "**Mechanical Vibrations - Theory and application to structural dynamics**," 2nd ed., John Wiley & Sons, New York (**1997**).

[17] Parton V.Z., and Kudryavtsev B.A., "**Electromagnetoelasticity**," Gordon and Breach Science Publisher, New York (**1988**).

[18] Gatti P.L., and Ferrari V., "**Applied Structural and Mechanical Vibrations: Theory, Methods and Measuring Instrumentation**," **1999**, E & FN Spon, Taylor and Francis Group, London.

[19] Liberatore, S., "**Analytical redundancy, fault detection and health monitoring for structures**," Ph.D Thesis, University of California, Los Angeles, CA, Dec. **2002**.

[20] Durga P. Malladi and Jason L. Speyer, "**A generalized shiryayev sequential probability ratio test for change detection and isolation**," *IEEE Transactions on Automatic Control*, vol. AC-44, no. 8, pp.1522-1534, Aug. **1999**.

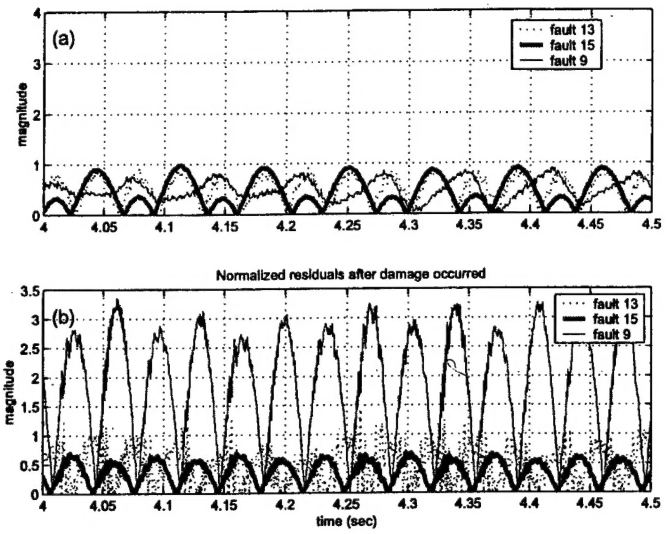

(a) Filter $N°1$

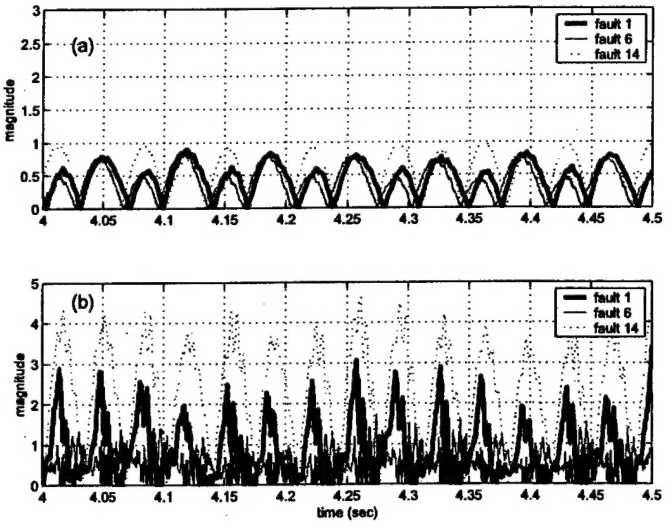

(b) Filter $N°4$

Figure 11: Measured data. Filter N^o 1 and Filter N^o 4. Normalized norms of the projected residuals: A) Before damage and B) after damage